GEOPHYSICS, VOL. 83, NO. 2 (MARCH-APRIL 2018); P. B47–B57, 10 FIGS.
10.1190/GEO2017-0110.1

Case History

Mapping chromite deposits with audio magnetotellurics in the Luobusa ophiolite of southern Tibet

Lanfang He[1], Ling Chen[2], Dorji[3], Zhanxiang He[4], Xuben Wang[5], Bayi Xiao[4], Ligui Xu[4], Xuefang Zhao[6], Xiaolu Xi[6], Hongchun Yao[6], and Rujun Chen[6]

ABSTRACT

The exploration of podiform chromites in the Indus Yarlong Zangbo suture zone of southern Tibet has proved difficult because most known deposits pinch out and then reappear in the same direction. Several ground-based geophysical approaches such as gravity, magnetic, and controlled-source audio-frequency magnetotelluric (CSAMT) methods have been applied to explore for these chromite deposits but have mostly failed to delineate prospective areas. We have evaluated a successful podiform chromite exploration case history that is based on AMT. More than 8000 AMT stations were used in this study within a 10 km^2 area of the ophiolite belt. Line separations were 80 or 40 m, and the station separation was 20 m. We implemented Bostick conversion and nonlinear conjugate gradient inversions for data interpretation, whereas 2D resistivity sections and 3D resistivity imaging were used to elucidate the inner structure and distribution of rock faces within the Luobusa ophiolite. Results from rock physics and drilling further indicate that resistivity-anomaly domains from these AMT results are correlated with rock faces in terms of fresh harzburgite, altered harzburgite and dunite, and they can thus be connected to concealed deposits. Therefore, we have developed three resistivity-anomaly models for chromite exploration, and we delineated several prospective regions containing exploitable deposits within the Luobusa ophiolite. Seven of the nine verified boreholes discussed in this paper intersected with chromite deposits; one comprises the largest and highest grade chromite deposit in China to date. Our AMT results provide the impetus for future chromite exploration in Tibet and enable a refined understanding of the structure and distribution of rock faces within the Luobusa ophiolite.

INTRODUCTION

The Luobusa ophiolite is part of the eastern portion of the Yarlung Zangbo ophiolite, which is controlled by the Indus-Yarlung Zangbo suture zone that separates Eurasia from the Indian continent in southern Tibet (Figure 1). Significant progress has been made in recent years toward an understanding of the geologic characteristics of this ophiolite, including the geologic ages of constituent rock units,

First presented at the SEG Global Meeting: International workshop and gravity, electrical, and magnetic methods and their applications, Chenghu, China, 19–22 April 2015. Manuscript received by the Editor 23 February 2017; revised manuscript received 21 August 2017; published ahead of production 08 December 2017; published online 13 February 2018.

[1]State Key Laboratory of Lithospheric Evolution, Institute of Geology and Geophysics, Chinese Academy of Sciences, Beijing, China; Key Laboratory of Seismic Observation and Geophysical Imaging, Institute of Geophysics, CEA, Beijing, China and State Key Laboratory of Mineral Deposits Research, School of Earth Sciences and Engineering, Nanjing University, Nanjing, China. E-mail: mofoo@263.net.
[2]State Key Laboratory of Lithospheric Evolution, Institute of Geology and Geophysics, Chinese Academy of Sciences, Beijing, China and CAS Center for Excellence in Tibetan Plateau Earth Sciences, Beijing, China. E-mail: lchen@mail.iggcas.ac.cn.
[3]Tibet Bureau of Exploration and Development of Geology and Mineral Resources, Lhasa, China. E-mail: duoj@cae.cn.
[4]BGP, China National Petroleum Corporation, Zhuozhou, China. E-mail: hezhanxiang@bgp.com.cn; xiaobayi@cnpc.com.cn; xuligui@bgp.com.cn.
[5]State Key Laboratory of Oil and Gas Reservoir Geology and Exploitation, Chengdu University of Technology, Chengdu, China. E-mail: wxb@cdut.edu.cn.
[6]Key Laboratory of Metallogenic Prediction of Nonferrous Metals and Geological Environment Monitoring, Ministry of Education; Key Laboratory of Non-Ferrous Resources and Geological Hazard Detection, School of Geosciences and Info-Physics, Central South University, Changsha, China. E-mail: cohhen@163.com; bgpmofo@yahoo.com; chrujun@csu.edu.cn.

its environment of formation, and the regional tectonics of southern Tibet (Pan et al., 2002; Côté et al., 2005; Zhou et al., 2005; Yin, 2006; Royden et al., 2008; Wu et al., 2014; Wang et al., 2015; Hu et al., 2016). The Luobusa ophiolite is important because it contains the largest reservoir of chromite in China, encompassing almost 90% of the total national production (Wang et al., 2010; Bao et al., 2014). Systematic exploration and studies have been carried out on the Luobusa ophiolite since the initial discovery of chromite in 1956 (Zhang et al., 1996). Much of the studies have focused on the mineralogy, lithology, economic geology, and features of this deposit, as well as the tectonics and the origin of these podiform chromites (Wang and Bao, 1987; Zhang et al., 1996; Zhou et al., 1996, 2005, 2014; Yang et al., 2003, 2007, 2014; Bao et al., 2014; Xu et al., 2015). However, several key characteristics of this ophiolite still remain under debate, including its tectonic occurrence, mechanism of emplacement, nature of the interior of the rock body, and location of favorable areas for mining (Liang et al., 2011; Li et al., 2012, Li et al., 2016; He et al., 2014). The origin of this rock body and the nature of the chromite are also debated; Zhou et al. (1996, 2005) and Zhou and Robinson (1997) develop a melt-rock reaction model for the Luobusa podiform chromite. Bao et al. (2014) use the occurrence of highly depleted mantle peridotites and a high chromite content to suggest that this ophiolite formed in a forearc basin environment. Research by Yang et al. (2007, 2014) and Yamamoto et al. (2009) also supports a deep mantle origin for the Luobusa podiform chromites.

In spite of research progress on the origins and basic geology of podiform chromites, the exploration for concealed deposits has proved problematic (Frasheri, 2009). Geophysical methods have been used to search for orebodies and to map geologic structures to study the factors controlling the mineralization (Frasheri, 2009). Because of density and magnetic-susceptibility differences between an orebody and its host rocks, gravity and magnetic methods have been widely applied since the 1940s for chromite exploration (Hammer, 1945; Hammer et al., 1945; Yüngül, 1956; Davis et al., 1957; Wu, 2006; Frasheri, 2009). Ten percent of the interpreted anomalies have been verified as buried chromite deposits within the Bulqiza ultrabasic massif in Albania (Frasheri, 2009). Progress has recently been achieved in the use of gravity and magnetic processing and the inversion methods for exploration (José et al., 2007; Liu et al., 2012; Mandal et al., 2013; Qiu, 2013; He et al., 2014). A range of additional geophysical methods, including induced polarization (IP) and magnetotellurics (MTs), has also been used for indirect chromite exploration (Xi et al., 2013; Jiang et al., 2015); however, the geologic conditions under which podiform chromite deposits occur are complex and remain incompletely understood; the physical and chemical properties of chromite do not lend themselves easily to the indirect prospecting methods commonly applied to other ores, such as zinc or copper (Kospiri, 1999). Therefore, individual geophysical methods exhibit several limitations that negatively impact their applicability at specific sites. Integrated surveys comprising gravity, magnetic, and IP approaches, as well as MT methods, are usually used in podiform chromite exploration. In some cases, these integrated approaches have led to the discovery of significant ore deposits and have yielded information about host rock structure (Kospiri, 1999; Mohanty et al., 2011; Jiang et al., 2015). Mohanty et al. (2011) present a case study in which they use a range of integrated geologic and geophysical approaches including gravity, magnetic, electrical, and electromagnetic (EM) methods to delin-

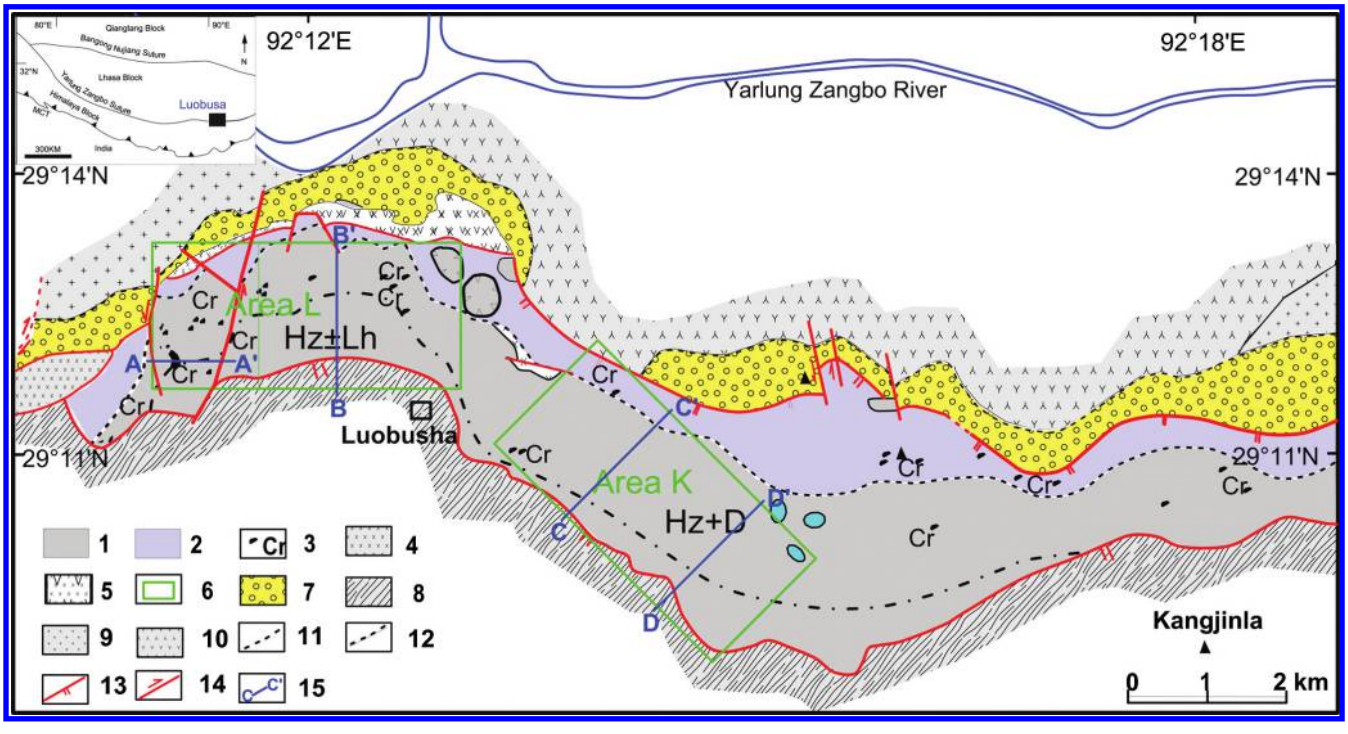

Figure 1. Schematic geologic map of the Luobusa ophiolite (He et al., 2014, modified after Li et al., 2012). The black filled rectangle at the top left corner shows the location of the working area in Tibet. The legends are 1, harzburgite (bearing dunite and lherzolite); 2, dunite; 3, chromites ore; 4, cumulus bojite; 5, cumulus consisting of bojite, wehrlite; 6, scope of the surface magnetic survey; 7, Luobusa group conglomerate; 8, upper Triassic Formation; 9, quartz diorite, quartz monzonite; 10, biotite granite; 11, lithostratigraphic boundary; 12, unconformable contact; 13, reverse fault; 14, strike-slip fault; 15, section and its position.

eate chromite deposits. The results of that study indicate that, compared with the use of any single geophysical technique, the systematic integration of complementary geophysical methods reduces the ambiguity in interpretation. Between 2009 and 2011, Jiang et al. (2015) surveyed multiple exploration profiles around the Luobusa ophiolite using seismic reflection, MT, controlled-source audio-frequency MT, gravity, and magnetic methods to investigate the origin of chromites and to prospect for other deposits in the area. The results of that study provided key data on the deep structure of the Luobusa ophiolite and revealed the presence of mantle upwelling material within the Yarlung Zangbo suture zone.

A limited amount of geophysical exploration has been conducted over the past century in the Luobusa ophiolite and its vicinity. Previous investigations have applied gravity and magnetic (Wu, 2006), IP (Qu, 1978), and borehole EM (Fu and Jiang, 1986) methods in this region, but the results were unconvincing to geologists because only a few ore deposits have been discovered by drilling based on the geophysical interpretations. Because a few concealed ore deposits were nevertheless discovered over the past 30 years via drilling exploration based on geologic analysis (Wang et al., 2010), exploration for chromite has become a key challenge in Luobusa. To explore for and evaluate concealed and potential chromite deposits within the Luobusa ophiolite, we conducted a comprehensive exploration project financed by mining companies between 2012 and 2013. We applied detailed gravity, magnetic, AMT, and IP methods using spread spectrum technology (Xi et al., 2013) over a 10 km^2 area within the ophiolite region to search for chromite (He et al., 2015). AMT and IP were the major geophysical exploration methods applied in this project; we identified several favorable areas and located many economic chromite deposits via exploratory drill cores. One drill core that was based on an AMT result with a nonlinear conjugate gradient (NLCG) inversion interpretation resulted in the discovery of four layers of chromite with a total thickness of 49.18 m, the largest deposit found so far in China. We discuss our field operations, data processing, and AMT results in this paper and report correlations with the occurrence of chromite deposits. We also discuss the applicability of AMT models in chromite exploration.

GEOLOGIC SETTING

The chromite deposits within the Luobusa ophiolite are associated with Alpine-type peridotites, one of the various assemblages within the Yarlung Zangbo ophiolite belt (Pan et al., 2002), distributed in an east–west direction over approximately 2000 km in southern Tibet. Our study area (Figure 1) comprises a small but vital part of a major tectonic contact within the Yarlung Zangbo ophiolite belt, one of the most known and most extensively studied of the ophiolites in China (Wu et al., 2014). The Luobusa ophiolite is approximately 40 km in length and ranges in width between 0.7 and 4 km; this ophiolite covers an area of approximately 70 km^2 and has a general east–west trend. A suite of island-arc volcanic-rock sequences is located immediately to the north of the Luobusa ophiolite, discordantly overlain by polymictic and sandy conglomerates of the Tertiary Luobusa group (Zhang et al., 1996; Bao et al., 2014). To the south, this ophiolite has a faulted contact with Upper Triassic turbidites, and some Cretaceous intermediate-acid magmatic rocks are also present in the study area (Bao et al., 2014). Based on available outcrop observations and drill-core results, the major lithotypes within the Luobusa ophiolite are identified as harzburgite and dunite (Figure 1). The contact between these two lithotypes is characterized as the central ore-bearing zone, and most of the chromite appears to occur within, or close to, this zone. Based on results presented by Wu et al. (2014), the age of ophiolite host rock emplacement has been dated as approximately 130 Ma.

The Luobusa ophiolite is composed of metamorphic mantle peridotite, mafic-ultramafic cumulate, and gabbro or diabase dikes. More than 93% of this ophiolite is made up of metamorphic mantle peridotite, and altered rocks include serpentine and magnetite; this mantle peridotite mainly consists of dunite (orthorhombic pyroxene, OPX < 10%), OPX-poor harzburgite (OPX 10%–25%), and harzburgite (OPX > 25%). The major elemental constituents of chromites in the podiform chromites and mantle peridotites in the Luobusa ophiolite were reported by Zhang et al. (1996) and Zhou et al. (1996). These data show that the molar ratio of forsterite (Fo, $Fo = 100\ Mg/(Mg + Fe)$) in the host ophiolite ranges between 88% and 94%, and it is between 93.6% and 96.4% in the chromite deposits. The average Cr_2O_3 mass content is between 0.75% and 0.90% in enstatite, 1.04% in clinopyroxene, and 1.07% in lherzolite, but it is only 0.67% in dunite. Two major assemblages characterize the Luobusa ophiolite: an upper part containing dunite-harzburgite and OPX-poor harzburgite (mostly containing lenses of dunite and some large-scale, high-grade chromite deposits) and a lower part that consists of a harzburgite-lherzolite complex subzone (sometimes containing dunite and lherzolite with chrome diopside levels between 4% and 5%, up to occasionally between 7% and 8%) (Bao et al., 2014). The transition band between these two major assemblages plays an important role in high-grade chromite exploration, and its burial depth ranges from several tens of meters to several hundreds of meters. The presence of high-grade deposits is also controlled by faults that generally strike from west to east. Most of the known chromite deposits are podiform and pinch out and reappear in the same direction, creating issues for geologic and geophysical exploration (Zhang et al., 1996).

METHODS

AMT was the dominant method we used for comprehensive podiform chromite exploration within the Luobusa ophiolite. This natural, or passive, source EM method has played an important role in the search for concealed chromite deposits and uses naturally occurring MT fields within the audio-frequency band 10 Hz to 10 kHz to investigate the electrical-conductivity structure of the earth's near surface. The natural sources of AMT are thunderstorms occurring worldwide because energy discharged by lightning emits EM fields that propagate over great distances. AMT fields at the earth's surface behave like plane waves (Vozoff, 1991), and are measured as orthogonal electric (E) and magnetic (H or B) fields (Figure 2). Frequency-based impedance results, which correspond to the distribution of electrical conductivity in the subsurface, can therefore be acquired from the amplitude, phase, and directional relationships between surface electric and magnetic fields (Vozoff, 1991; Asch and Sweetkind, 2011).

We conducted a high-density AMT survey at more than 8000 stations across a 10 km^2 area within the Luobusa ophiolite belt (area L and area K in Figure 1). The line spacing was 80 or 40 m, and the normal station spacing was 20 m. Survey line directions were laid out across the strike of the ophiolite belt; in the western part of area L, survey lines were laid from west to east (A-A′ in Figure 1). In the eastern part of this area, survey lines were laid out from south to north (B-B′ in Figure 1). In contrast, all the survey

lines within area K trend from the southwest to northeast with an azimuth of 42° (C-C′ and D-D′ in Figure 1). We used 4 MTU-5A sets (Phoenix Geophysics) and 20 PMT-2 sets (an AMT receiver developed by Champion Geophysics) MT receiver units for data acquisition, recording horizontal electric and magnetic fields in two orthogonal directions (Ex, Ey, Hx, and Hy in Figure 2), along the trend of the survey line (the *x*-direction), as well as across the survey line (the *y*-direction). The normal E dipole lengths used to measure the Ex and Ey electric fields were 20 m, corresponding to the separation between Ex0 and Ex1 (or between Ey0 and Ey1) in Figure 2. We also used five PbCl-Pb electrodes, two pairs for the Ex and Ey dipoles, and a fifth electrode for central ground contact. A pair of coils is used to measure the orthogonal components of the magnetic field at each station. The measured time-series signals are first converted to complex cross spectra using the fast Fourier transform (FFT). Tensor apparent resistivities and phases are derived from the complex cross spectra by robust cross spectral analysis (He et al., 2006; Sampson and Rodriguez, 2010). We acquired apparent resistivities and phases at each station for 40 frequencies ranging between 11.5 and 11,250 Hz. More than 90% of our AMT data were of high quality (Figure 3a and 3b), and the remaining 10% of data were of low quality as shown in Figure 3c. No remote references were used for data processing. Most stations used a mutual reference comparing their data with the magnetic data from another array; the average acquisition duration was greater than 30 min.

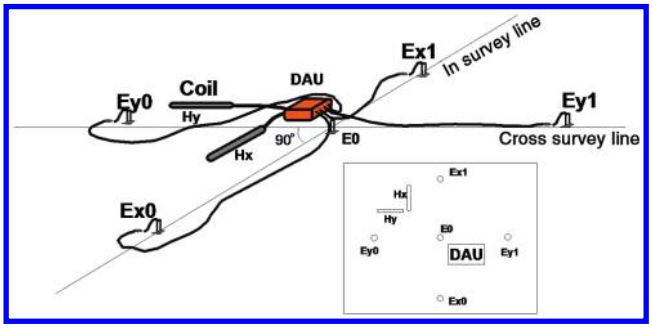

Figure 2. Field layout of AMT data acquisition. The horizontal electric and magnetic fields are recorded in two orthogonal directions (Ex, Ey, Hx, and Hy). In general, the *x*-direction is along the trend of the survey line and the *y*-direction is across the survey line. The normal E dipole length, the separation between Ex0 and Ex1 (or Ey0 to Ey1), is 20 m. Data are acquired by the data acquisition unit (DAU). E0 is the central ground contact point in the center of this survey station.

We used the software package SSMT2000 (Phoenix Geophysics) for onsite data processing, including preconditioning the time-series data by verifying or editing site parameters and specifying FFT times, converting from the time to frequency domain, calculating impedance estimates (Share et al., 2014), and correcting them using calibration data from acquisition boxes and coils. We then used the MTeditor (part of the SSMT2000 package) to evaluate calculated impedances and response curves (Asch and Sweetkind, 2011; Share et al., 2014). Other data processing included editing and static-shift correction. The first of these processes involved the removal of individual cross-powers from the calculations to enable poor-quality data to be edited; this was accomplished by marking poor-quality cross-powers (which normally have large deviations) with a noncommercial program. In the case of data containing artifactual noise, we selected cross-powers referring to adjacent frequencies or stations.

We used EM array profiling (EMAP) filtering (Torres-Verdin and Bostick, 1992) as a postprocessing step to correct topographic and static shifts in the data along the survey line direction (*xy*) before inversion or conversion. The EMAP approach uses a low-pass filter to diminish topographic and static-shift effects in the spatial or wavenumber domains. A filter constant *c* that performs the role of a window-width expansion factor in an applied Hanning window is used as part of the adaptation process to control roll-off characteristics (Torres-Verdin and Bostick, 1992). The filter constant *c* can be set within a range between zero and five, where zero indicates no EMAP filtering, whereas a value greater than five indicates that all the data will be smoothed flat with little lateral prediction. Wang et al. (2017) outline a detailed discussion and comparison of the effects of the filter constant *c*; we applied a value between 0.1 and 0.4 for Luobusa ophiolite data processing and interpretation, in concert with Bostick conversion (for a detailed discussion of this approach and comparison to other inversion methods, see Bostick, 1977; Wang et al., 2017). NLCG inversion based on the algorithm of Rodi and Mackie (2001) was applied for AMT data inversion. We set a noise floor of 5% in NLCG for the resistivity and phase. The iterations we used were between 12 and 15 and a root-mean-square (rms) value that ranged between 4.5 and 6.6. Some stations have skin depths of less than 400–800 m, and the inversion results of

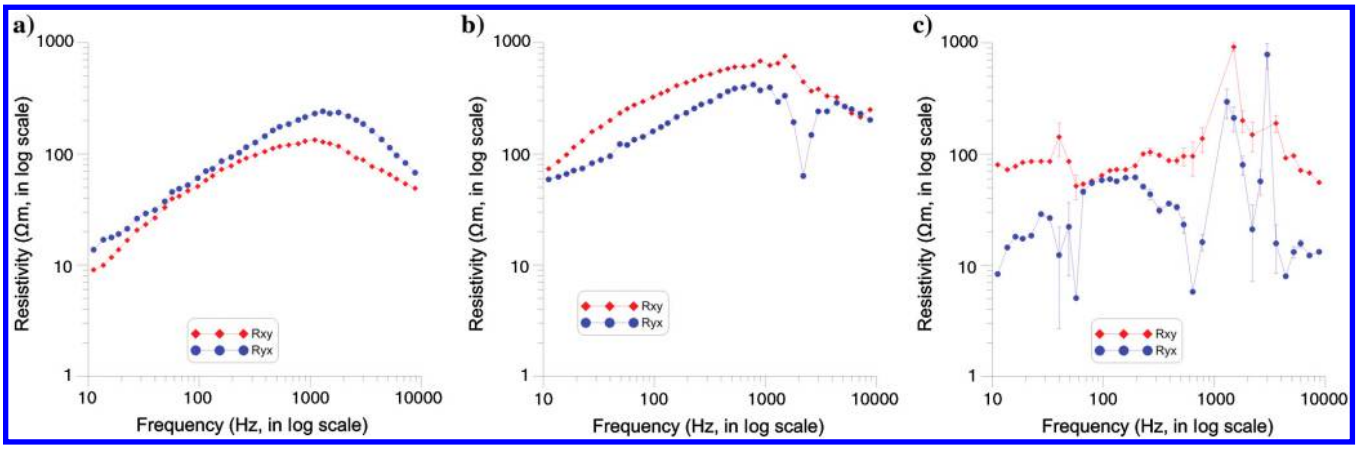

Figure 3. Examples of the typical resistivity curves for (a) high-quality data, (b) normal, and (c) low-quality data.

these stations shown in the figures have been blanked. A comparison of a raw data section (section AA′ as shown in Figure 1) with modeling results from the 2D inversion is shown in Figure 4; the number of NLCG iterations is 15 in this case with an rms of 6.56%. Figure 4a and 4c shows resistivity and phase of the raw data from the section of 56 stations with 20 m station separation. Each AMT data in one station encompasses 40 frequencies ranging between 11.20 and 10,040 Hz. Figure 4b and 4d shows those of the modeling results based on the inversion model of the section. Apart from the phase, these raw and modeled data profiles exhibit similar geoelectrical properties, which indicates that the inversion is reasonable.

AMT is widely used in mine and engineering geophysics. In most cases, we have no or few geologic data in the working or study areas, so the result of the AMT is the only knowledge before digging or drilling. The methods we used to decrease the uncertainty includes comparing the result of different inversion or conversion methods; comparing to results from other geophysical methods; comparing to the known mine deposits, caves, or faults; and testing the modeling data. The best way is comparing the result to drillholes. In some areas of Luobusa, we have geologic and borehole data, so we can verify the inversion model and get a set of "reasonable" parameters for conversion or inversion. In some other areas of the Luobusa rock mass, we have no geologic data because of a lack of coverage or other reasons. In these areas, the depth of the target can only be inferred from the AMT inversion model. The parameters we used are from the verified section. We set a uncertainty of 20% or more when we propose a drillhole base on the AMT model, and then we set a target depth (e.g., 80–120 m) for drilling.

RESULTS AND DISCUSSION

Rock physics

To better understand the electrical properties of the ultramafic rocks within the Luobusa ophiolite, we measured the complex impedance of the natural samples under dry conditions, which means that the samples did not undergo a soaping process, at room temperature, and at atmospheric pressure. We measured all samples using a four-pole electrode system configuration, encompassing two outer current and two inner potential electrodes (He et al., 2016). Complex resistivity measurements were performed using a Solartron-1260A impedance/gain-phase analyzer, and the range of frequencies used for impedance spectroscopy was between 0.005 and 1000 Hz. We measured a total of 75 samples from the Luobusa ophiolite.

Our results show that sample resistivity varies from tens of Ωm up to 10 million Ωm, around a mean of 0.85 MΩm. Data show that 20% of our samples exhibited resistivities less than 10 kΩm, 45% had values between 10 and 1000 kΩm, and 35% had resistivities greater than 1000 kΩm (Figure 5a). Complex resistivity results for harzburgite (HAR), chromite (Cr), and dunite (DUN) samples are shown in Figure 5b. The data show that the resistivity of the harzburgite samples is approximately 100 MΩm across a frequency range between 0.005 and 10 Hz, and that the resistivity decreases sharply in concert with increasing frequencies higher than 10 Hz. The resistivity of the chromite samples is some 30 kΩm across the whole range of frequency measurements, between 0.005 and 1000 Hz, decreasing gradually as the frequency increases. The values for three dunite samples range from less than 100 to more than 100 kΩm, the resistivity low is mainly due to the serpentinization and their high free-water content (more than 8 wt%) measured in terms of loss on ignition. Fresh harzburgite samples have

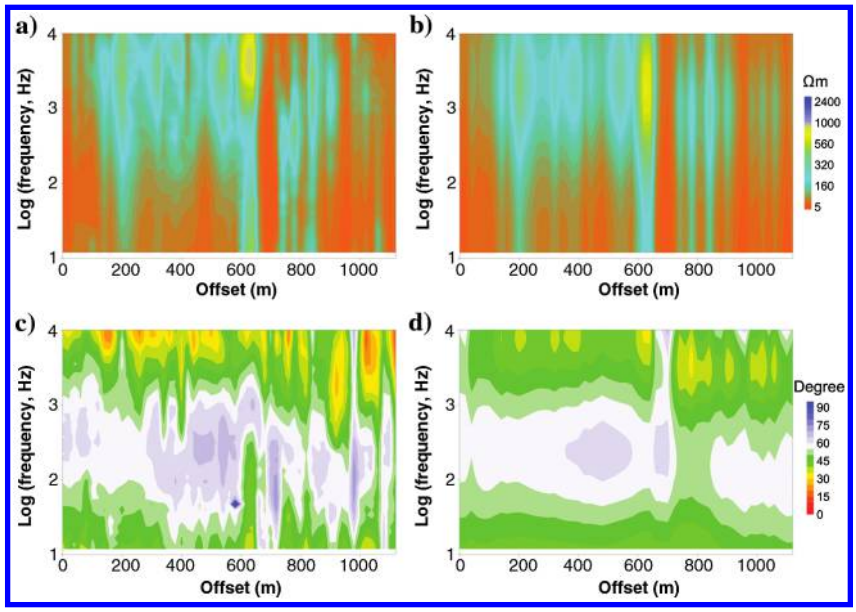

Figure 4. Comparison of the raw-data section (section AA′ as shown in Figure 1; it has 56 stations with 20 m station separation encompassing 40 frequencies ranging between 11.20 and 10,040 Hz) with modeling results from the 2D inversion. The iteration number of NLCG is 15 with an rms of 6.56%. (a and c) Resistivity and phase raw data from the section. (b and d) Those of the modeling results based on the inversion model of the section.

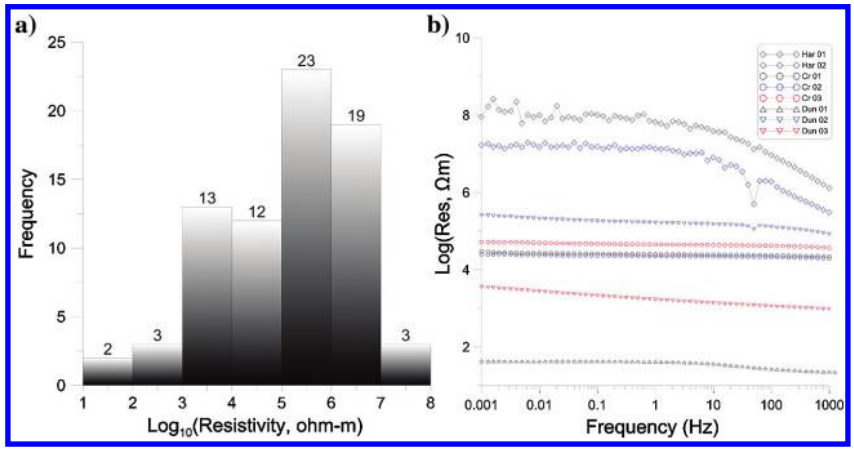

Figure 5. (a) Resistivity histogram and (b) complex resistivity of harzburgite (fresh), chromite, and dunite (fresh to serpentinized) of samples from the Luobusa ophiolite.

the highest resistivity, about four orders of magnitude higher than chromite.

2D section results

We collated AMT results from a survey of more than 100 profiles across our study to reveal significant internal structural details of the Luobusa ophiolite (all located in area L and area K, Figure 1). Inversion results from two typical AMT sections, B-B′ and C-C′, are shown in Figure 6 (see Figure 1 for their locations); these two sections can be generally divided into three domains based on the electrical responses: a top low-resistivity domain yielding values between 40 and 300 Ωm (d1), a middle domain (d2) yielding highly variable resistivity values between 300 and 3000 Ωm, and a deep-buried low-resistivity domain (d3) characterized by generally low-resistivity values between 10 and 200 Ωm.

In general, the resistivities from the laboratory samples (rock physics) have correlation to the resistivities of the formation or rock mass where the rocks were sampled, but the values are always different. First, in the laboratory, samples are directly measured, the value means "true" resistivity. But the resistivities interpreted from the AMT sections are calculated from the ground-measured electric and magnetic field, the value means the cross resistivities of the formation or rock mass. Second, the samples for laboratory measurements are sampled from the drill core, but the detritus and gouge, which greatly decrease the resistivity of the formation or rock mass, could not be measured in the laboratory. These made the resistivities from the laboratory samples to be several times even orders of magnitude higher than those interpreted from the AMT sections.

Section B-B′ (Figure 6a) is 1400 m in length and extends in a south to north direction. The top domain within this section is generally characterized by low-resistivity values between 40 and 300 Ωm and has a thickness ranging from 10 to 80 m. Conversion results show that resistivity values range between 40 and 80 Ωm in the interval, between 1100 and 1200 m in distance, and between 120 and 300 Ωm across the rest of this domain. This shallow domain is interpreted as indicative of loose Quaternary system deposits based on drill core and other geologic data. In contrast, the middle domain (d2) has a thickness of some 760 m in depth from 80 to 840 m (elevations from 4320 to 3560 m) and distance between 0 and 900 m from south to north, and it is characterized by highly variable resistivity values. This domain exhibits resistivities that are generally greater than 500 Ωm. A high-resistivity layer characterized by values greater than 1000 Ωm yields a maximum value of 3000 Ωm at its center. Drill-core and rock-physics results indicate that this high-resistivity layer mainly comprises fresh harzburgite, and that the transitions within this domain that have a range of resistivities between 500 and 1000 Ωm consist of altered (partially serpentinized) harzburgite and dunite. The third and deepest domain (d3) occurs at depths approximately 800 m and at an elevation of lower than 3560–3600 m at a distance from 0 to 900 m. At distances greater than 900 m, its top interface goes up to elevation 4050 m with a depth of some 200 m. This domain is characterized by very low-resistivity values between 10 and 200 Ωm as well as having a southern-dipping gradient in resistivity values at an apparent dip of approximately 60°. Based on drill core and rock physics results, this very low-resistivity domain is thought to be indicative of altered dunite, which contains more than 8 wt% water content.

Section C-C′ (Figure 6b) is 1600 m in length, trends from the southwest to northeast, and it is situated in the northwest Luobusa ophiolite area K (Figure 1). Although this section is characterized by an EM response similar to that seen in section B-B′, the top domain (d1) is divided into three parts by its high-resistivity counterpart (d2). The data show that the thickness of d1 (the top layer) in this section ranges from less than 10 m to approximately 80 m. It reflects the loose Quaternary system deposits as in section B-B′. The middle domain (d2) within this section is characterized by highly variable resistivity values that range between 300 and 3000 Ωm, and it is between 100 and 700 m in thickness. Four blocks with re-

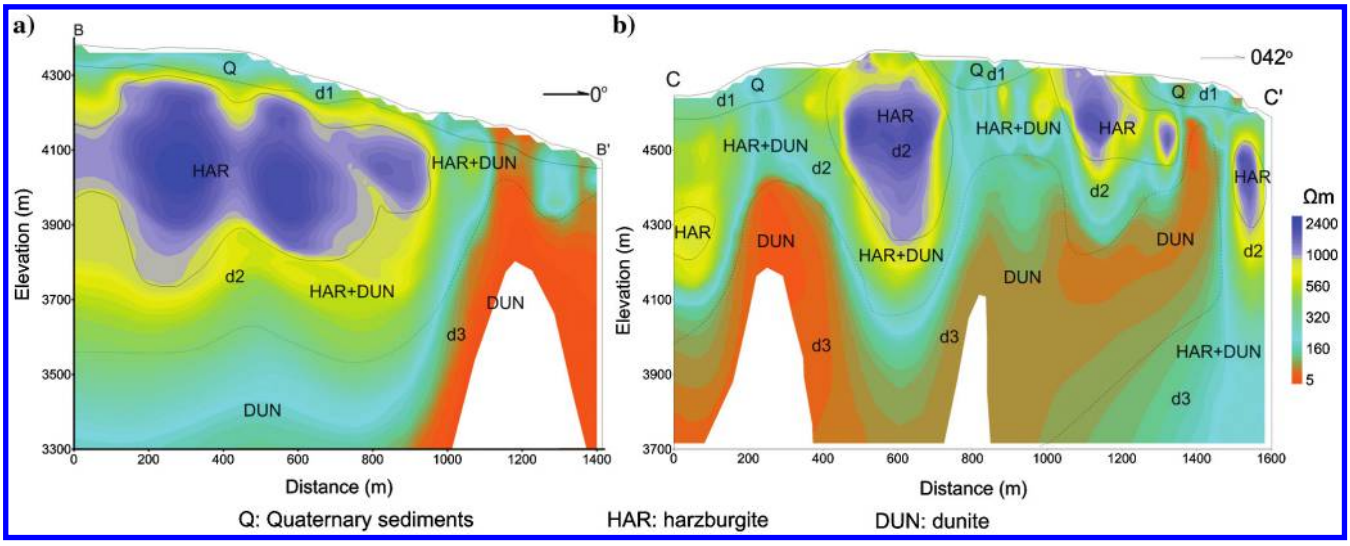

Figure 6. Typical resistivity cross section from the AMT results of the different portions of the Luobusa ophiolite: (a) from the middle portion of area L and (b) from area K. The result shows that the rock mass could generally be divided in three domains: a shallow low-resistivity domain (d1) reflects the loose deposits of the Quaternary systems, a middle domain (d2) has highly variable resistivity value from 300 to 3000 Ωm due to fresh harzburgite and the altered harzburgite and dunite, and a very low-resistivity deep domain (d3) of the altered dunite with high water content. The white blanked area means that there are no convertion data due to the lower skin depth at that station.

sistivities greater than 1000 Ωm are developed at distances of 60, 600, 1200, and 1550 m; they are interpreted as fresh harzburgite. Results and observations from drill cores, mine tunnels, and rock physics suggest that the transitions within this domain are indicative of altered harzburgite and dunite. The deep very low-resistivity domain (d3) within this section is characterized by a generally southwest and flat-dipping gradient less than 30°. Similar to section B-B′, this domain reflects altered dunites and also has a high water content.

3D view of AMT results

We performed 3D imaging analysis using 2D converted data from each section using commercial scientific visualization software. The resultant 3D view of our AMT results reflects the electrical properties of the internal structure and rock faces distribution of the entire Luobusa ophiolite rock mass. Three-dimensional resistivity image results for area K are shown in Figure 7. Figure 7a illustrates face-render results from rock mass that have resistivities higher than 800 Ωm. Figure 7b illustrates those that have resistivities less than 50 Ωm. From the surface to a depth of 1500 m, the rock mass in area K can be divided generally into a higher resistivity upper domain and a lower resistivity basal domain. A continuous and thin high-resistivity block that yields values greater than 800 Ωm trends from the northwest to southwest across area K (Figure 7b); this high-resistivity block is more than 3000 m in length and is interpreted as fresh harzburgite, controlling the distribution of chromite deposits. Another similar and discontinuous thin high-resistivity block with comparable properties trends from the northwest to southeast, and both are characterized by burial depths that range between 50 and 700 m. Results show that the dominant domain characterizing area K of the Luobusa ophiolite exhibits resistivities less than 100 Ωm and that most of the rock masses of this type have burial depths greater than 400 m. The low-resistivity (less than 50 Ωm) volume within the upper section of the ophiolite has been divided into three parts by two slender and high-resistivity blocks (Figure 7b). Rocks characterized by lower resistivity values are interpreted as mainly altered dunite. The rest of the ophiolite is characterized by resistivities that range from 50 to 800 Ωm intermediate between high-resistivity blocks and low-resistivity volume. They are reflections of partially serpentinized harzburgite and dunite. Most of the chromite deposits occur within this transitional zone.

The relationship between AMT results and chromite deposits

Understanding the relationship between the AMT results and the location of the chromite deposits is of paramount exploration importance because chromite deposits occur within the transition zone between harzburgite and dunite (Zhang et al., 1996; Zhou et al., 2005; Wang et al., 2010). Our research is therefore a major step forward because we are able to elucidate this relationship via correlations between the AMT results and rock faces (Figure 8) in concert with rock-physics results (Figure 5). The data presented in Figure 8a reveal the relationship between a known chromite deposit and the resistivity cross section. A 6 m thick chromite deposit occurs within the transition zone between higher-resistivity (fresh harzburgite) and lower-resistivity domains (serpentinized harzburgite and dunite). On this basis, we propose the use of a "transition zone" model (T model) for chromite exploration. This model is characterized by a high-resistivity upper domain with values higher than 800–1000 Ωm (fresh harzburgite), a region of low resistivity lower than 50–100 Ωm with a thickness greater than 100 m (serpentinized dunite), and a transitional domain with intermediate values (100–800 Ωm). We carried out a comprehensive exploration in Luobusa, so we can use some other data such as gravity, magnetic, and spectral IP method to help to guide the drilling. But the AMT model is the dominant foundation for proposing drilling. Comparing our exploration result to the AMT model (with known deposits) shown in Figure 8a and referring to the gravity and magnetic results, we proposed drilling based on this model within the section shown in Figure 8b. Drill cores within this area intersected a new chromite deposit that has a maximum thickness of 49.18 m, including two thin sheets of rock with a total thickness of approximately 3 m. This level of success based on model predictions provides further evidence that the chromite deposits occur mostly within transitional resistivity zones, although the reasons for this, as well as how these zones control the formation and size of deposits, remain unclear and

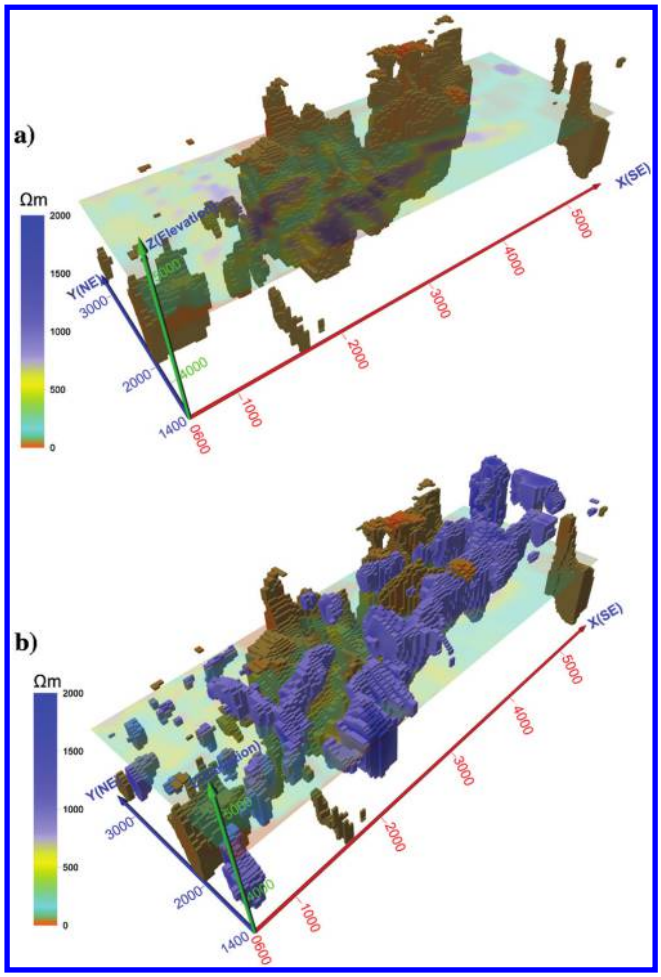

Figure 7. Three-dimensional resistivity view of area K at Luobusa ophiolite based on AMT inversion data. The result is imaged by commercial 3D scientific visualization software using 2D converted data from each section. (a) The face-render results of the rock mass with resistivity lower than 50 Ωm, which reflects altered dunite. (b) Those of the resistivity higher than 800 Ωm, which mainly reflect fresh harzburgite and its relation to the lower-resistivity rock mass.

are under study. We also present two additional chromite exploration models based on the resistivity results discussed in this study. The first of these is called the "lower resistivity fracture" model (F model) in which a deposit is characterized by low resistivity and occurs in an ophiolite fracture (Figure 8c), especially relatively shallow ones. According to this model, chromite is always found at the boundary and sometimes in the middle of the ophiolite. Most of the drill cores targeting this model encountered thin, small-scale deposits. The second of our two additional models is referred to as the "lower resistivity entrapment" model (E model) in which a deposit is characterized by low resistivity (Figure 8d), enclosed by high-resistivity host rocks. The model is widely applied across the northern region of the Luobusa ophiolite, and it is consistently related to the occurrence of medium- to small-scale deposits.

Between 2012 and 2013, nine proposed boreholes were drilled to verify chromite AMT exploration results. Of these, two are consistent with the T model, and both intersected high-grade deposits. One of them, borehole 02 (Figure 8b), led to the discovery of the largest and highest-grade Chinese chromite deposit to date. Five additional boreholes were drilled on the basis of the E model, and four intersected chromite deposits with thicknesses ranging between 0.6 and 5.6 m, and the fifth did not intersect any minerali-

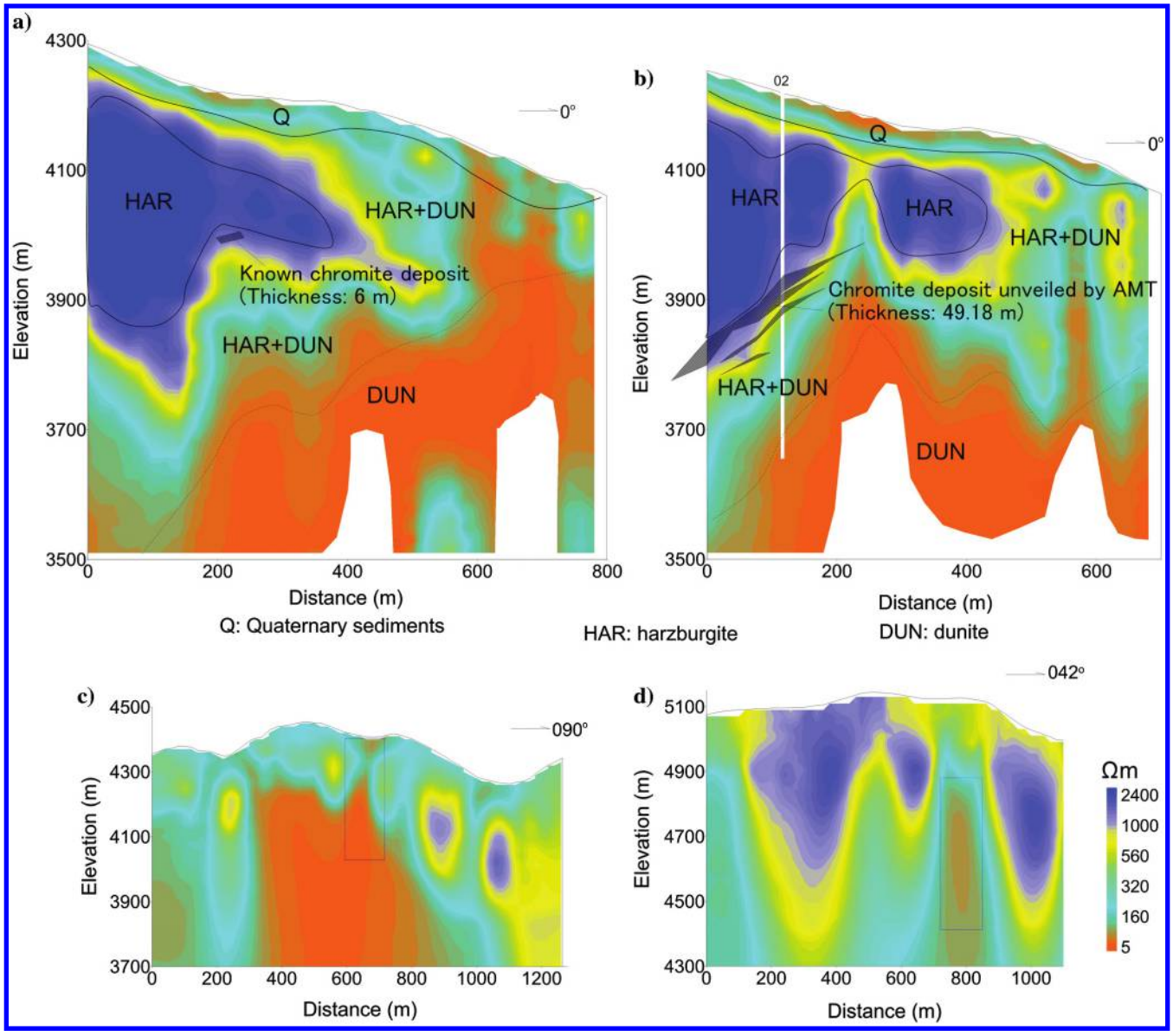

Figure 8. Relationship between the resistivity domain and the chromite deposit in the AMT section. (a) The relationship between a known deposit with a thickness of 6 m and the resistivity cross section in area L. The deposit lies in the transition zone from the higher resistivity domain (the fresh harzburgite) to a lower resistivity domain (the serpentinized harzburgite and dunite). (b) The location of our proposed borehole and deposit unveiled by the Borehole 02 in area L. The extension of the deposit was outlined by other drills. (a and b) An example of the transition zone model (T model) for chromite exploration. (c) Referred to as the lower-resistivity fracture model (F model) and (d) reflect the lower-resistivity entrapment model (E model).

zation. Finally, two boreholes were drilled on the basis of the F model, and one of them intersected a thin deposit.

Between 2014 and 2015, several drillholes intersected chromite deposit in area K. Figure 9 shows the results of two drillholes. Figure 9a and 9b shows the proposed target burial depth and the depth of the deposit unveiled by drillholes (X01 and X02) in different section. The chromite deposits lie lower than the proposed elevation. X01 shows that the deposit lies in the transition between high-resistivity and low-resistivity domain. X02 shows that the deposit lies in the low-resistivity domain. X03 is a proposed drillhole, but the drill has not been carried out. These two sections indicated the chromite deposits have lower burial depth than our proposed target depth, and in this area, the host rocks have a lower resistivity than those in area L.

Conception model of the Luobusa ophiolite

Research and exploration on the Luobusa ophiolite has been ongoing for several decades (Zhang et al., 1996; Wu 2006; Wang et al., 2010; Bao et al., 2014). The structure underlying area L has been considered to conform to a model described by a southward-dipping "monoclinal structure" (Figure 10a) based on results from some drill cores as well as other geologic and geophysical interpretations (Zhang et al., 1996; Wang et al., 2010; Jiang et al., 2015). On the basis of this interpretation, chromite deposits in the southern portion of area L (Figure 10a) are very hard to exploit because they are likely to have been buried at elevations lower than 3500 m, corresponding to depths between 800 and 900 m, the same as the water level in the Yarlung Zangbo River. However, our AMT results reveal that the internal structure of the Luobusa ophiolite in fact differs from this previously applied monoclinal structure model. Our results show (Figure 10b) that in the area, the chromite-bearing layer (a cumulate mixtite layer containing harzburgite, dunite, and the chromite deposit) discovered AMT (the blue rectangle), from the south to north, within this ophiolite is in fact consistent with a "drape structure" model because it undulates from the north to south. In other words, the rock faces zone (i.e., the ductile shear belt, or mixtite) is uplifted to the south of area L. Therefore, we conclude a drape structure model to map the structure of the Luobusa ophiolite where AMT could reach. This model has important implications for our understanding of the inner structure of the Luobusa ophiolite as well as for chromite deposit exploration. Based on this model, the southern portion of the Luobusa ophiolite should be considered a new prospective area and the drillholes have found exploitable chromite deposits there.

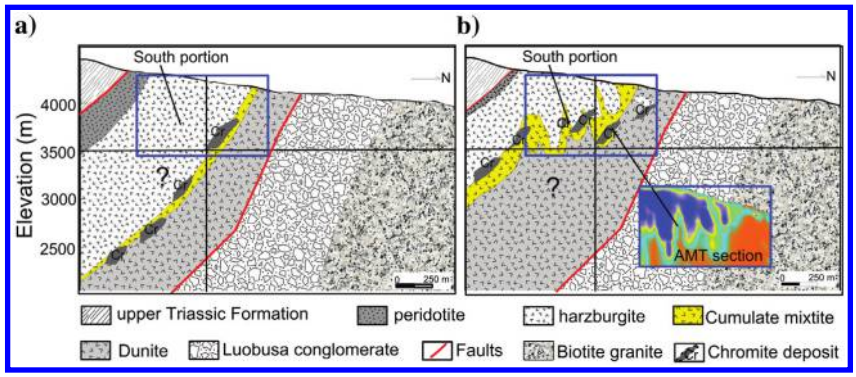

Figure 10. (a) Conventional conception model and (b) model based on the AMT result of the inner structure of the Luobusa ophiolite. The conventional model on the structure of the ophiolite under area L was considered to be a southward-dipping monoclinal structure model (a) based on the results of some drilling and the other geologic and geophysical interpretations. We proposed a new conception model as shown in (b), from south to north, the chromite bearing layer in the ophiolite is a drape structure; it goes up and down from north to south. The model in the blue rectangle is from the result of the AMT section; the rest is from the conventional conception.

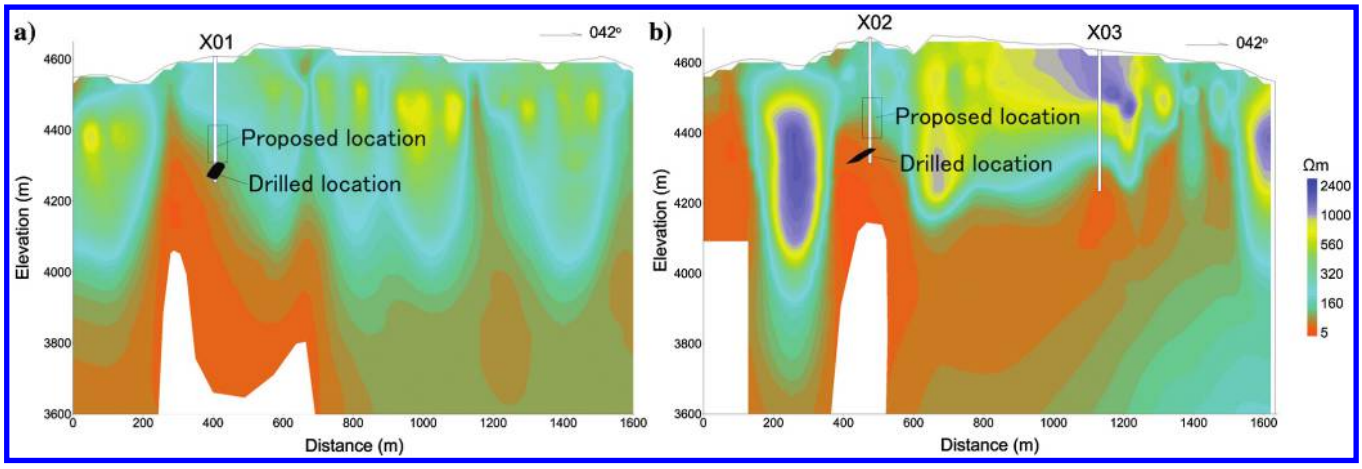

Figure 9. Relationship between the resistivity domain and the chromite deposit in the AMT section of area K. (a and b) The proposed target location and drilled location of the mine in different section and drillholes (X01 and X02). The chromite deposits lies under the proposed location. X01 shows that the mine lies in the transition of high-resistivity and low-resistivity domain. X02 shows that the mine lies in the low-resistivity domain. X03 is the proposed drillhole, but the drilling has not been carried out.

CONCLUSION

We presented a case study of applying AMT to explore for deeply buried podiform chromite within the Luobusa ophiolite of southern Tibet. We surveyed more than 100 AMT sections across the whole rock mass with lengths between 1400 and 1600 m and with a station separation of 20 m. Typical sections of the Luobusa ophiolite combined with a 3D view of our AMT results showed that this rock mass can generally be divided into three domains: a shallow low-resistivity region that is indicative of loose Quaternary system deposits; a middle domain characterized by highly variable resistivity values between 300 and 3000 Ωm due to the presence of fresh harzburgite, altered harzburgite and dunite; and a deep very low resistivity domain interpreted as altered dunite with a high water content. Our results also reveal that different parts of the Luobusa ophiolite have significantly different geoelectric properties. Thus, correlations between AMT anomalies and rock faces provided a new way to understand the relationships between resistivity distributions and the occurrence of chromite deposits.

Therefore, we proposed three resistivity models for future chromite exploration that are based on correlations among AMT, known deposits, and drilling results. Our proposed models are effective, and the largest chromite deposit in China to date has been uncovered by boreholes based on our approach. The AMT results showed that the internal structure of the Luobusa ophiolite is different from the previously proposed monoclinal structural model. The interfaces between the different rock faces within this ophiolite do not entirely dip to the south, but they undulate from south to north. Our results have led to the discovery of new favorable areas for chromite exploration within the Luobusa ophiolite. Data from AMT surveys also significantly refine our understanding of the structure and distribution of rock faces within the Luobusa ophiolite.

ACKNOWLEDGMENTS

We thank M. D. Wang and Gepin for their assistance with this project, as well as Jiangnan Mining for providing drill core data. This research was supported by the Strategic Priority Research Program (B) of the Chinese Academy of Sciences (XDB03010800), the National Natural Science Foundation of China (41774083, 41274078), and the Chinese Geological Survey (DD20160193, 12120113095200).

REFERENCES

Asch, T. H., and D. S. Sweetkind, 2011, Audiomagnetotelluric characterization of range-front faults, Snake Range, Nevada: Geophysics, **76**, no. 1, B1–B7, doi: 10.1190/1.3511358.

Bao, P. S., S. Li, J. Wang, and Q. G. Zhai, 2014, Origin of the Zedang and Luobusa Ophiolites, Tibet: ACTA Geologia Sinica (English Edition), **88**, 669–698, doi: 10.1111/1755-6724.12222.

Bostick, F. X., 1977, A simple almost exact method of MT analysis *in* S. H. Word, Workshop on electrical methods in geothermal exploration, Snowbird, Utah: U.S. Geological Survey Contract 14-08-001-6-359, 174–183.

Côté, D. V., R. Hébert, C. Dupuis, C. S. Wang, Y. L. Li, and J. Dostal, 2005, Petrological and geochemical evidence for the origin of the Yarlung Zangbo ophiolites, southern Tibet: Chemical Geology, **214**, 265–286, doi: 10.1016/j.chemgeo.2004.10.004.

Davis, W. E., W. H. Jackson, and D. H. Richter, 1957, Gravity prospecting for Chromite deposits in Camaguey province, Cuba: Geophysics, **22**, 848–869, doi: 10.1190/1.1438427.

Frasheri, A. I., 2009, The peculiarities of geophysical methods in exploration for chrome deposits: 79th Annual International Meeting, SEG, Expanded Abstracts, 1310–1314.

Fu, H. D., and J. G. Jiang, 1986, Test result of borehole radiowave penetration method in the Xianggeshan chromite ore district, Tibet (in Chinese with English abstract): Geophysical and Geochemical Exploration, **10**, 57–60.

Hammer, S., 1945, Estimating ore masses in gravity prospecting: Geophysics, **10**, 50–62, doi: 10.1190/1.1437147.

Hammer, S., L. L. Nettleton, and W. K. Hastings, 1945, Gravimeter prospecting for chromite in Cuba: Geophysics, **10**, 34–49, doi: 10.1190/1.1437146.

He, L. F., L. Chen, X. F. Zhao, R. J. Chen, and W. L. Li, 2016, Electromagnetism of ultramafic rocks from the Luobusa ophiolite studied at room temperatures and pressures, *in* Q. Y. Di, ed., Resource detection and environmental protection with applied geophysics: Atlantis Press, 45–48, doi: 10.2991/iceeg-16.2016.13.

He, L. F., M. H. Feng, Z. X. He, and X. B. Wang, 2006, Application of EM methods for the investigation of Qiyueshan Tunnel, China: Journal of Environmental and Engineering Geophysics, **11**, 151–156, doi: 10.2113/JEEG11.2.151.

He, L. F., X. M. Hu, Y. B. Zha, L. G. Xu, and Y. H. Wang, 2014, Distribution and origin of high magnetic anomalies at Luobusa Ophiolite in Southern Tibet: Chinese Science Bulletin, **59**, 2898–2908, doi: 10.1007/s11434-014-0330-6.

He, L. F., X. M. Hu, X. F. Zhao, and R. J. Chen, 2015, Podiform chromite exploration using audio magnetotelluric at Luobusa Ophiolite in Southern Tibet: International Workshop and Gravity, Electrical & Magnetic Methods and their Applications, 314–317.

Hu, X. M., E. Garzanti, J. G. Wang, W. Huang, W. An, and A. Webb, 2016, The timing of India-Asia collision onset — Facts, theories, controversies: Earth-Science Reviews, **160**, 264–299, doi: 10.1016/j.earscirev.2016.07.014.

Jiang, M., M. Peng, J. S. Yang, H. D. Tan, R. Y. Qian, Y. W. Zhang, L. H. Xu, L. S. Zhang, and Q. Q. Li, 2015, Seismic reflection and magnetotelluric profiles across the Luobusa ophiolite: Evidence for the deep structure of the Yarlung Zangbo suture zone, southern Tibet: Journal of Asian Earth Sciences, **110**, 4–9, doi: 10.1016/j.jseaes.2015.03.019.

José, A. B. R., M. A. Pérez-Flores, Q. G. Gerardo, and L. A. Gallardo, 2007, Geometry of ophiolites in eastern Cuba from 3D inversion of aeromagnetic data, constrained by surface geology: Geophysics, **72**, no. 3, B81–B91, doi: 10.1190/1.2712425.

Kospiri, A., 1999, Integrated geophysical surveys for searching of podiform chromite in Albania: 69th Annual International Meeting, SEG, Expanded Abstracts, 354–357.

Li, J. Y., J. S. Yang, D. Z. Ba, X. Z. Xu, F. C. Meng, and T. F. Li, 2012, Origin of different dunites in the Luobusa ophiolite at Luobusa ophiolite, Tibet (in Chinese with English abstract): Acta Petrologica Sinica, **28**, 1829–1845.

Li, X. H., F. Mattern, C. K. Zhang, Q. G. Zeng, and G. Z. Mao, 2016, Multiple sources of the Upper Triassic flysch in eastern Himalaya orogen, Tibet, China: Implications to paleogeography and paleotectonic evolution: Tectonophysics, **666**, 12–22, doi: 10.1016/j.tecto.2015.10.005.

Liang, F. H., Z. Q. Xu, D. Z. Ba, and Y. Jia, 2011, Tectonic occurrence and emplacement mechanism of ophiolites from Luobusa-Zedang, Tibet (in Chinese with English abstract): Acta Petrologica Sinica, **27**, 3255–3268.

Liu, T. Y., Y. S. Yang, J. X. Liu, J. C. Gou, and B. H. Su, 2012, The effects of using high-precision gravity and magnetic methods to explore chromite in the Xiugou iron deposit, Langxian County, Tibet (in Chinese with English abstract): Geophysical and Geochemical Exploration, **36**, 325–331.

Mandal, A., W. K. Mohanty, and S. P. Sharma, 2013, 3D compact inverse modeling of gravity data for chromite exploration — A case study from Tangarparha, Odisha, India: 83rd Annual International Meeting, SEG, Expanded Abstracts, 1171–1174.

Mohanty, W. K., A. Mandal, S. P. Sharma, G. Saibal, and M. Surajit, 2011, Integrated geological and geophysical studies for delineation of chromite deposits: A case study from Tangarparha, Orissa, India: Geophysics, **76**, no. 5, B173–B185, doi: 10.1190/geo2010-0255.1.

Pan, G. T., X. Z. Li, L. Q. Wang, J. Ding, and Z. L. Chen, 2002, Preliminary division of tectonic units of the Qinghai-Tibet Plateau and its adjacent regions: Geological Bulletin of China, **21**, 701–707.

Qiu, L. Q., 2013, The effect of applying the electromagnetic wave CT to the exploration of the Norbusa chromite ore district in Tibet (in Chinese with English abstract): Geophysical and Geochemical Exploration, **37**, 59–63.

Qu, D. X., 1978,Chromite exploration using induced polarization (in Chinese with English abstract): Northwestern Geology, **11**, 93–99.

Rodi, W., and R. L. Mackie, 2001, Nonlinear conjugate gradients algorithm for 2-D magnetotelluric inversion: Geophysics, **66**, 174–187.

Royden, L. H., B. C. Burchfiel, and D. Robert, 2008, The geological evolution of the Tibetan plateau: Science, **321**, 1054–1058, doi: 10.1126/science.1155371.

Sampson, J. A., and B. D. Rodriguez, 2010, Audio-magnetotelluric survey to characterize the Sunnyside porphyry copper system in the Patagonia Mountains, Arizona: U.S. Geological Survey, Open-File Report 2010-1311, 1–5.

Share, P. E., A. G. Jones, M. R. Muller, D. T. Khoza, M. P. Miensopust, and S. J. Webb, 2014, An audio-magnetotelluric investigation of the Otjiwarongo and Katima Mulilo regions, Namibia: Geophysics, **79**, no. 4, B151–B171, doi: 10.1190/geo2013-0171.1.

Torres-Verdin, C., and F. X. Bostick, 1992, Principles of spatial surface electric field filtering in magnetotellurics: Electromagnetic array profiling (EMAP): Geophysics, **57**, 603–622, doi: 10.1190/1.1443273.
Vozoff, K., 1991, The magnetotelluric method, in M. N. Nabighian, ed., Electromagnetic methods in applied geophysics: vol. 2 Applications Part B: SEG, Investigations in Geophysics 3, 641–711.
Wang, E. Q., J. J. K. Peter, G. Q. Xu, K. V. Hodges, K. Meng, L. Chen, G. Wang, and H. Luo, 2015, Flexural bending of southern Tibet in a retro foreland setting: Scientific Reports, **5**, 12076, doi: 10.1038/srep12076.
Wang, X. B., and P. S. Bao, 1987, The genesis of podiform chromite deposits-a case history of the Luobusa chromite deposit, Tibet (in Chinese): Acta Geologica Sinica, **61**, 166–181.
Wang, X. B., X. Zhou, and Z. G. Hao, 2010, Some opinions on further exploration for chromite deposits in the Luobusa area, Tibet, China (in Chinese with English abstract): Geological Bulletin of China, **29**, 105–114.
Wang, X. J., L. F. He, L. Chen, L. G. Xu, J. Li, X. Y. Lei, and D. H. Wei, 2017, Mapping deeply buried karst cavities using controlled-source audio magnetotellurics: A case history of a tunnel investigation in southwest China: Geophysics, **82**, no. 1, EN1–EN11, doi: 10.1190/geo2015-0534.1.
Wu, F. Y., C. Z. Liu, L. L. Zhang, C. Zhang, J. G. Wang, W. Q. Ji, and X. C. Liu, 2014, Yarlung Zangbo ophiolite: A critical updated view (in Chinese with English abstract): Acta Petrologica Sinica, **30**, 293–325.
Wu, Q., 2006, A Study on the prospecting direction and method of chromium deposit in Xizang (Tibet) (in Chinese with English abstract): Shanghai Geology, **27**, 58–63.
Xi, X. L., H. C. Yang, L. F. He, and R. J. Chen, 2013, Chromite mapping using induced polarization method based on spread spectrum technology: Symposium on the Application of Geophysics to Engineering and Environmental Problems, 13–19.
Xu, X. Z., J. S. Yang, P. T. Robinson, F. H. Xiong, D. Z. Ba, and G. L. Guo, 2015, Origin of ultrahigh pressure and highly reduced minerals in podiform chromites and associated mantle peridotites of the Luobusa ophiolite, Tibet: Gondwana Research, **27**, 686–700, doi: 10.1016/j.gr.2014.05.010.
Yamamoto, S. J., T. Komiya, K. Hirose, and S. Maruyama, 2009, Coesite and clinopyroxene exsolution lamellae in chromites: In-situ ultrahigh-pressure evidence from podiform chromites in the Luobusa ophiolite, southern Tibet: Lithos, **109**, 314–322, doi: 10.1016/j.lithos.2008.05.003.
Yang, J. S., W. J. Bai, Q. S. Fang, B. G. Yan, N. C. Shi, Z. S. Ma, M. Q. Dai, and M. Xiong, 2003, Silicon-rutile — An ultrahigh pressure (UHP) mineral from an ophiolite: Progress in Natural Science, **13**, 528–531.
Yang, J. S., L. Dobrzhinetskaya, W. J. Bai, Q. S. Fang, P. T. Robinson, J. F. Zhang, and H. W. Green, 2007, Diamond-and coesite-bearing chromites from the Luobusa ophiolite, Tibet: Geology, **35**, 875–878, doi: 10.1130/G23766A.1.
Yang, J. S., P. T. Robinson, and Y. Dilek, 2014, Diamonds in ophiolites: Elements, **10**, 127–130, doi: 10.2113/gselements.10.2.127.
Yin, A., 2006, Cenozoic tectonic evolution of the Himalayan orogen as constrained by along-strike variation of structural geometry, exhumation history, and foreland sedimentation: Earth-Science Reviews, **76**, 1–131, doi: 10.1016/j.earscirev.2005.05.004.
Yüngül, S., 1956, Prospecting for chromite with gravimeter and magnetometer over rugged topography in east Turkey: Geophysics, **21**, 433–454, doi: 10.1190/1.1438245.
Zhang, H. Y., D. Z. Ba, T. Y. Guo, X. X. Mo, J. Z. Xue, P. Y. Ruan, and Y. Z. Wang, 1996, Research of Luobusa chromite deposit in Qusong, Tibet (in Chinese): Tibet Press.
Zhou, M. F., and P. T. Robinson, 1997, Origin and tectonic environment of podiform chromite deposits: Economic Geology, **92**, 259–262, doi: 10.2113/gsecongeo.92.2.259.
Zhou, M. F., P. T. Robinson, J. Malpas, S. J. Edwards, and L. Qi, 2005, REE and PGE geochemical constraints on the formation of dunites in the Luobusa ophiolite, Southern Tibet: Journal of Petrology, **46**, 615–639, doi: 10.1093/petrology/egh091.
Zhou, M. F., P. T. Robinson, J. Malpas, and J. W. Li, 1996, Podiform chromites in the Luobusa ophiolite (southern Tibet): Implications for melt-rock interaction and chromite segregation in the upper mantle: Journal of Petrology, **37**, 3–21, doi: 10.1093/petrology/37.1.3.
Zhou, M. F., P. T. Robinson, B. X. Su, J. W. Li, J. S. Yang, and J. Malpas, 2014, Compositions of chromite, associated minerals, and parental magmas of podiform chromite deposits: The role of slab contamination of contamination of asthenospheric melts in supersubduction zone environments: Gondwana Research, **26**, 262–283, doi: 10.1016/j.gr.2013.12.011.